

# Rossby Wave Propagation from the Arctic into the Midlatitudes: Does It Arise from In Situ Latent Heating or a Trans-Arctic Wave Train?

TINGTING GONG

*CAS Key Laboratory of Ocean Circulation and Waves, Institute of Oceanology, Chinese Academy of Sciences, and Pilot National Laboratory for Marine Science and Technology (Qingdao), and Center for Ocean Mega-Science, Chinese Academy of Sciences, Qingdao, China*

STEVEN B. FELDSTEIN AND SUKYOUNG LEE

*Department of Meteorology and Atmospheric Science, The Pennsylvania State University, University Park, Pennsylvania*

(Manuscript received 13 November 2018, in final form 27 November 2019)


## ABSTRACT

The relationship between latent heating over the Greenland, Barents, and Kara Seas (GBKS hereafter) and Rossby wave propagation between the Arctic and midlatitudes is investigated using global reanalysis data. Latent heating is the focus because it is the most likely source of Rossby wave activity over the Arctic Ocean. Given that the Rossby wave time scale is on the order of several days, the analysis is carried out using a daily latent heating index that resembles the interdecadal latent heating trend during the winter season. The results from regression calculations find a trans-Arctic Rossby wave train that propagates from the subtropics, through the midlatitudes, into the Arctic, and then back into midlatitudes over a period of about 10 days. Upon entering the GBKS, this wave train transports moisture into the region, resulting in anomalous latent heat release. At high latitudes, the overlapping of a negative latent heating anomaly with an anomalous high is consistent with anomalous latent heat release fueling the Rossby wave train before it propagates back into the midlatitudes. This implies that the Rossby wave propagation from the Arctic into the midlatitudes arises from trans-Arctic wave propagation rather than from in situ generation. The method used indicates the variance of the trans-Arctic wave train, but not in situ generation, and implies that the variance of the former is greater than that of latter. Furthermore, GBKS sea ice concentration regression against the latent heating index shows the largest negative value six days afterward, indicating that sea ice loss contributes little to the latent heating.

## 1. Introduction

Observations have shown that the Arctic surface air temperature (SAT) has undergone a larger warming trend during recent decades compared to that in the midlatitudes (e.g., Chapman and Walsh 1993; Serreze et al. 2009; Bekryaev et al. 2010; Lee et al. 2011; Cohen et al. 2014), especially during winter. This phenomenon has been commonly referred to as Arctic amplification. A number of recent studies suggest that associated with

Arctic amplification there has been a large-amplitude response in the midlatitudes due to the loss of sea ice (e.g., Deser et al. 2007, 2016; Overland and Wang 2010; Francis and Vavrus 2012, 2015; Screen and Simmonds 2013; Cohen et al. 2014; Vihma 2014; Walsh 2014; Woollings et al. 2014; Overland et al. 2015; Sun et al. 2016). One leading hypothesis is that when sea ice melts, an upward surface heat flux (latent plus sensible heat) is followed by an excitation of Rossby waves that propagate from the Arctic into the midlatitudes through the troposphere, thereby influencing midlatitude weather (e.g., Budikova 2009; Honda et al. 2009; Deser et al. 2010; Overland and Wang 2010; Alexander et al. 2010). To excite these Rossby waves, there must be vortex tube stretching in the free atmosphere (i.e., above the

 Denotes content that is immediately available upon publication as open access.

Corresponding author: Tingting Gong, ttg@qdio.ac.cn

DOI: 10.1175/JCLI-D-18-0780.1

© 2020 American Meteorological Society. For information regarding reuse of this content and general copyright information, consult the [AMS Copyright Policy \(www.ametsoc.org/PUBSReuseLicenses\)](https://www.ametsoc.org/PUBSReuseLicenses).

atmospheric boundary layer) due to the release of latent heat. Therefore, an implicit assumption in the above hypothesis is that sea ice melting is followed by either 1) latent heat release in the air above the boundary layer or 2) an upward sensible heat flux that increases the vertical temperature gradient, which may destabilize the air column, resulting in convection and latent heat release. Either way, the implicit assumption of the above theory is that the resulting release of latent heat excites the equatorward propagation of Rossby waves. It has also been proposed that planetary-scale Rossby waves excited by latent heat release associated with sea ice melting in the Arctic follow a pathway upward from the troposphere into the stratosphere. These planetary waves constructively interfere with the climatological stationary waves, resulting in an enhanced poleward heat transport, followed by a weakening of the stratospheric polar vortex, and the excitation of streamfunction anomalies in the middle- and high-latitude troposphere via the process of downward control (e.g., [Feldstein and Lee 2014](#); [Kim et al. 2014](#); [Peings and Magnusdottir 2014](#)).

As shown in [Takaya and Nakamura \(2001\)](#), sources of Rossby wave activity arise from nonconservative processes (i.e., diabatic heating and friction). The excitation of Rossby waves is expected to be overwhelmingly due to diabatic heating (friction being primarily a sink and not a source of Rossby wave activity), which is dominated by latent heat release via convective heating and/or large-scale condensational heating. Sources of in situ (local to the Arctic) latent heat release in the atmosphere can occur through many different processes, such as 1) an upward surface latent heat flux due to sea ice loss and 2) an upward surface sensible heat flux due to sea ice loss as described above, 3) warm temperature advection near the surface (the latter two processes can destabilize the flow resulting in convection), and 4) large-scale condensational heating within Arctic cyclones. All of the above processes (including sea ice melting) are associated with latent heating and can therefore potentially excite Rossby waves that propagate equatorward from the Arctic into midlatitudes.

The possibility described above (i.e., that Rossby waves in the Arctic are triggered by latent heating) is plausible in principle, but given that the Arctic boundary layer is known to be very stable, especially in winter ([Serreze et al. 1992](#); [Persson et al. 2002](#)), it would be challenging for the surface heat fluxes to have such a substantial impact in the free troposphere. From this perspective, an easier, more straightforward way to generate latent heating in the free atmosphere over the Arctic is through horizontal advection of warm, moist air from lower latitudes. In fact, [Sorokina et al. \(2016\)](#)

showed that the first empirical orthogonal function of the surface turbulent heat flux (latent plus sensible heat) (33% of the variance) over the Barents Sea is driven by the atmosphere and is largely unrelated to sea ice variability. This alternative pathway is consistent with another mechanism of Arctic warming that seems especially relevant in the Atlantic sector of the Arctic, including the Greenland, Barents, and Kara Seas (GBKS). In this mechanism, Rossby waves originating from outside of the Arctic contribute to the warming by transporting warm, moist air into the Arctic followed by an increase in downward infrared radiation (IR) at the surface ([Doyle et al. 2011](#); [Lee et al. 2011](#); [Woods et al. 2013](#); [H.-S. Park et al. 2015](#); [D.-S. Park et al. 2015](#); [Woods and Caballero 2016](#); [Gong and Luo 2017](#); [Gong et al. 2017](#); [S. Lee et al. 2017](#); [H.-J. Lee et al. 2017](#); [Ding et al. 2017](#); [Luo et al. 2019](#); [Zhong et al. 2018](#); [Alekseev et al. 2019](#)). Therefore, it is possible that Rossby waves that propagate from the midlatitudes into the Arctic, by transporting sensible heat and moisture into the region, hinder sea ice growth (or even melt sea ice) and at the same time release latent heat, which then strengthens the Rossby waves prior to their return back into the midlatitudes on the other side of the Arctic Ocean.

The focus of the current study is to address the question of whether the excitation of equatorward propagating Rossby waves from the Arctic into midlatitudes is due to the in situ generation of Rossby waves via latent heating through at least one of the above processes, or due to Rossby waves propagating from midlatitudes into the Arctic and then back into midlatitudes, being amplified by anomalous latent heat release as they pass through the Arctic. One method for addressing the above question is to diagnose the circulation and thermodynamic anomalies associated with anomalous latent heat release over the Arctic. We consider two scenarios. If we find that the Arctic latent heating is 1) preceded by Rossby wave propagation into the Arctic, 2) the spatial structure of the Arctic latent heating is consistent with it being generated by the poleward propagating Rossby wave train (i.e., the spatial structure of the anomalous Arctic latent heating resembles that of the anomalous moisture flux convergence associated with the poleward propagating Rossby waves), and 3) the Arctic latent heating is followed by equatorward Rossby wave propagation into midlatitudes, then the Arctic latent heating is not associated with in situ processes; that is, we can claim that none of the above processes, including Arctic sea ice loss, can be the main driver of the equatorward propagating Rossby wave train. On the other hand, if we find that 1) there is little or no poleward Rossby wave propagation from midlatitudes into the Arctic prior to the release of latent heat in the Arctic and 2) latent

heating within the Arctic is followed by equatorward Rossby wave propagation, then in situ Arctic latent heating is generating the equatorward Rossby wave propagation. However, with our approach, if the latent heating is generated by in situ processes, we cannot isolate which of the above processes excites the equatorward propagating Rossby waves; that is, Arctic sea ice loss could be one of the several possible processes that generates latent heat release and excites equatorward Rossby wave propagation.

The processes described above, which involve Arctic latent heating and Rossby wave propagation, take place on the intraseasonal time scale. In the present study, we link these intraseasonal time scale processes to interdecadal variability. This perspective is consistent with the findings of Woods and Caballero (2016), who showed that almost 50% of the interdecadal Arctic warming trend can be explained by an increase in the frequency of occurrence of intraseasonal warm, moist air intrusions, which increase the surface downward IR. In Gong et al. (2017, hereafter GFL), the analogous perspective was taken that a substantial fraction of the interdecadal trend in surface downward IR arises from the interdecadal trend in the frequency of intraseasonal surface downward IR fluctuations, in addition to a possible contribution to the trend associated with variability at longer time scales. This linkage between intraseasonal and interdecadal variability was obtained by using linear regression. In the present study, we focus on the interdecadal trend in latent heating, using the same approach as in GFL. The results of this study will be used to address the question of whether or not in situ Arctic latent heating has an impact in midlatitudes on the interdecadal time scale via the excitation of equatorward propagating Rossby waves.

In this study, a regression approach is used. Being regression, our findings present average behavior. The results to be presented suggest that equatorward Rossby wave propagation is typically associated with a trans-Arctic wave train, not with in situ processes within the Arctic. It is important to point out that our results do not preclude the possibility that sometimes in situ processes such as sea ice loss are followed by upward surface heat fluxes and then latent heating, which can generate equatorward Rossby wave propagation. The regression results that we present suggest that in situ generation of equatorward propagating Rossby waves must be sufficiently uncommon so as not to make an important contribution to the mean behavior.

## 2. Data

For this study, we use the European Centre for Medium-Range Weather Forecasts (ECMWF) interim

reanalysis (ERA-Interim) (Dee et al. 2011) and the Japanese 55-year Reanalysis (JRA-55) (Ebita et al. 2011; Kobayashi et al. 2015) datasets for the months of December, January, and February (DJF). The JRA-55 reanalysis is used because it provides daily, three-dimensional convective heating and large-scale condensational heating data. In the ERA-Interim dataset, these two diabatic heating terms are not provided separately; rather, they are summed together with vertical temperature diffusion. In a recent study of SAT anomalies associated with the North Atlantic Oscillation (NAO) (Clark and Feldstein 2020), it was found that composites of the sum of convective heating, large-scale condensational heating, and vertical temperature diffusion from the ERA-Interim dataset closely resemble the sum of the same three variables from the JRA-55 dataset. For all variables other than convective heating, large-scale condensational heating, and sea ice concentration (see below), such as surface air temperature, downward infrared radiation, surface heat flux, streamfunction, Rossby wave activity fluxes, and column integrated moisture flux convergence, we use data from the ERA-Interim reanalysis.

The vertical profile of the DJF climatological convective heating rate over the Arctic (from 60°N to the North Pole) shows positive values throughout the free troposphere (between 925 and 300 hPa, with a maximum value near 800 hPa) in both the zonal mean (Fig. 1a) and in the sector mean of 30°W–60°E, which covers the GBKS region (Fig. 1b). The DJF climatological large-scale condensational heating rate also shows positive heating in the troposphere poleward of 60°N, with two maxima, one located near the surface and the other in the middle troposphere near 600 hPa (Figs. 1c,d). Since the spatial patterns of the two heatings are similar over the Arctic, in this study the convective and large-scale condensational heating are analyzed by summing and vertically integrating the two heatings from 925 to 300 hPa.

For the ERA-Interim surface heat and radiative flux fields, daily accumulated values at time steps 3 and 6 for both 0000 and 1200 UTC are used. For both 0000 and 1200 UTC, time step 3 (step 6) corresponds to a forecasted accumulated flux 3 h (6 h) later. The differences between the time step 6 and time step 3 forecasted values are calculated, and these differences are divided by the time interval in seconds. This calculation yields the time-averaged forecasted fluxes over the time interval between steps 3 and 6. The 0000 and 1200 UTC forecasted fluxes are then averaged to give the surface heat and radiative flux values for that day. In this study, we follow the ERA-Interim sign convention that all downward surface heat and radiative fluxes are positive.

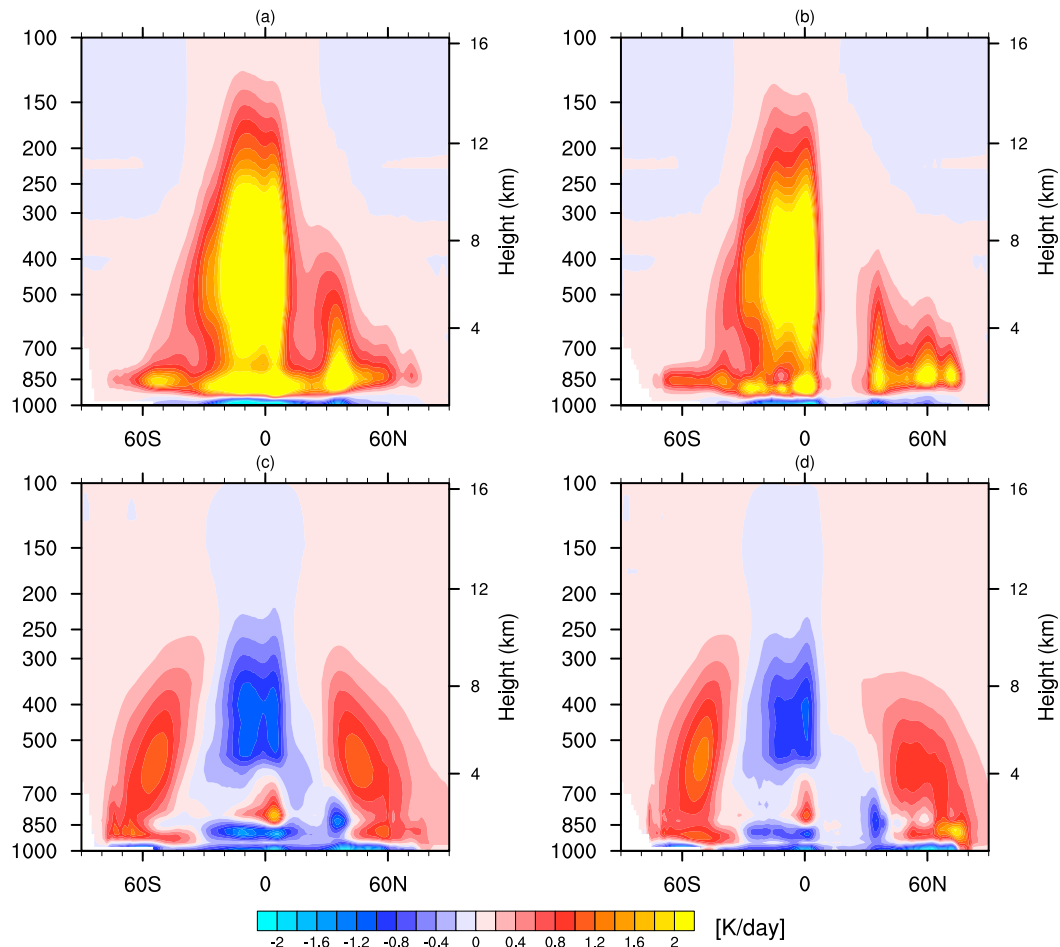


FIG. 1. The vertical profile of the December–February (DJF) climatological convective heating rate in the (a) zonal mean and (b) 30°W–60°E sector mean, and large-scale condensational heating rate in the (c) zonal mean and (d) 30°W–60°E sector mean (JRA-55 dataset).

For the sea ice data, we use the sea ice concentrations from *Nimbus-7* SMMR and DMSP SSM/I–SSMIS passive microwave data, version 1, from the National Snow and Ice Data Center (NSIDC) (Cavalieri et al. 1996).

### 3. Results

#### a. The latent heating rate trend over the Arctic

Before we investigate our hypothesis on the relationship between total latent heating (the sum of the convective and large-scale condensational heating from the JRA-55 dataset) in the GBKS region and poleward/equatorward Rossby wave propagation, we show the total latent heating rate trends ( $\text{W m}^{-2}$  per DJF winter season, hereafter referred simply to as latent heating) for the 15 consecutive 20-yr segments from the 1979–98 through 1993–2012 time period (Fig. 2). Over the Arctic Ocean, the first six segments of the earlier years exhibit a

weak negative trend, while the remaining nine segments of the later years show an accelerated positive trend over most of the Arctic. These trend patterns resemble the corresponding trends in SAT and downward IR for the same time period as in GFL. The strongest positive latent heating trend can be seen for the last segment (1993–2012) over the northern part of the GBKS region. During the same time segment, a strong negative latent heating trend can be seen between 30°W and 60°E, in the southern part of the GBKS region, and in the Norwegian Sea. Since both latent heating and latent cooling anomalies can excite Rossby waves and because, as we will see, the latent heating and cooling anomalies are dynamically linked, in this study we will focus on the domain 30°W–60°E, 60°–90°N for the 1993–2012 time period. Note that although the Greenland Sea, Barents Sea, and the Kara Seas extend to 80°N, for convenience we refer to 60°–90°N as the GBKS region.

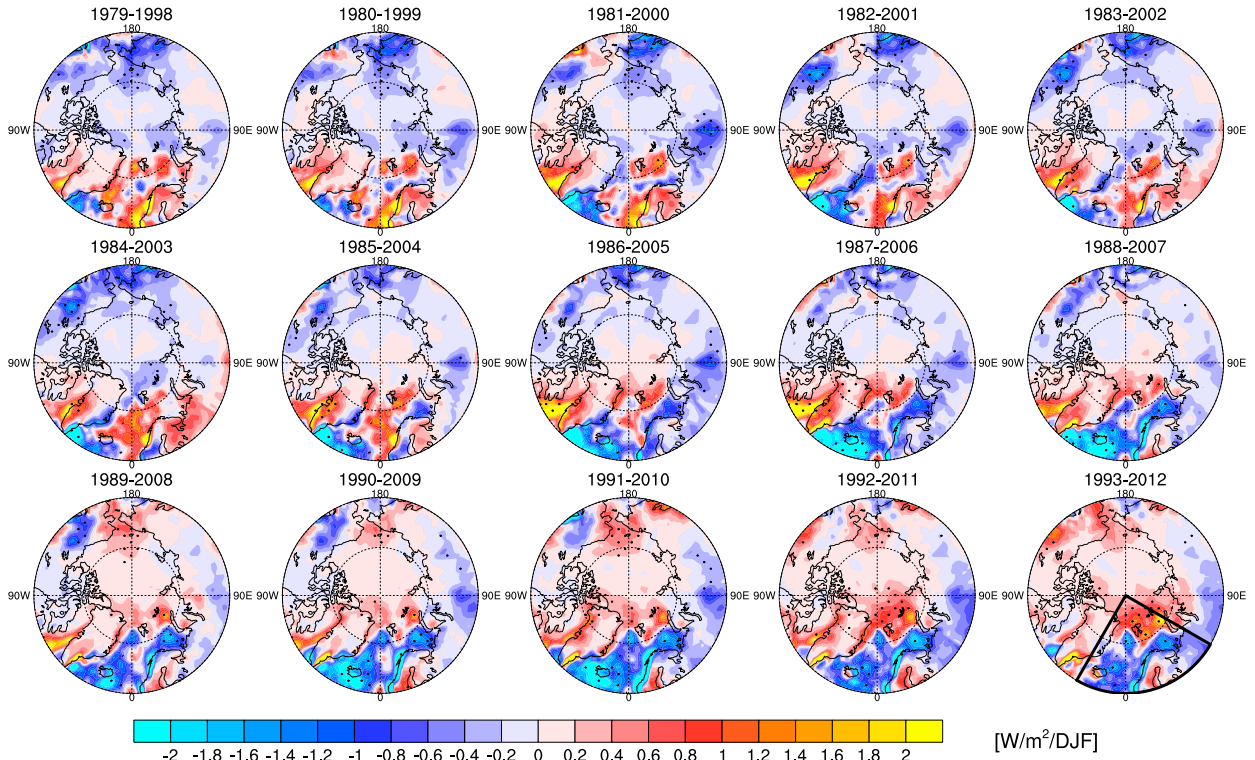


FIG. 2. The linear trends of the vertically integrated latent heating ( $\text{W m}^{-2}$ ; DJF winter season) for 15 different 20-yr time segments corresponding to the DJF winter seasons from 1979–98 through 1993–2012. The dots indicate values that are statistically significant at the  $p < 0.10$  level for a two-sided Student's  $t$  test (JRA-55 dataset).

### b. Downward IR, SAT, surface heat flux, and sea ice

To test our hypothesis on the relationship between latent heating in the Arctic and poleward/equatorward Rossby wave propagation, we have adopted the same method as in GFL, but applied it to the latent heating trend rather than surface downward IR trend. Following Feldstein (2003) and GFL, we first generate a daily latent heating index ( $H$  index) by projecting the daily latent heating field onto the 1993–2012 latent heating trend pattern in Fig. 2 for the domain of  $30^\circ\text{W}$ – $60^\circ\text{E}$ ,  $60^\circ$ – $90^\circ\text{N}$ . The daily latent heating can be written as

$$H(\lambda, \theta, t) = H_{\text{index}}(t)H_{\text{trend}}(\lambda, \theta) + H_r(\lambda, \theta, t), \quad (1)$$

where  $H(\lambda, \theta, t)$  is the daily latent heating field at longitude  $\lambda$ , latitude  $\theta$ , and time  $t$ , and  $H_{\text{trend}}(\lambda, \theta)$  is the observed 1993–2012 latent heating trend pattern shown in Fig. 2. On each day, the latent heating field has a contribution from the latent heating trend pattern  $H_{\text{trend}}(\lambda, \theta)$ , where the variable  $H_{\text{index}}(t)$  can be interpreted as corresponding to the amplitude of the latent heating trend pattern on each day, and from the daily residual latent heating  $H_r(\lambda, \theta, t)$ . As shown in Feldstein (2003),  $H_{\text{trend}}(\lambda, \theta)$  and  $H_r(\lambda, \theta, t)$  are spatially orthogonal to each other if  $H_{\text{index}}(t)$  is specified as

$$H_{\text{index}}(t) = \frac{\left[ \sum_{ij} H(\lambda, \theta, t) H_{\text{trend}}(\lambda, \theta) \cos\theta \right]}{\left[ \sum_{ij} H_{\text{trend}}(\lambda, \theta)^2 \cos\theta \right]}, \quad (2)$$

where  $i$  and  $j$  are the longitudinal and latitudinal grid points, respectively. We refer to  $H_{\text{index}}(t)$  as the  $H$  index. Figure 3 shows the time series of the  $H$  index for 1993–2012. As can be seen, this time series undergoes rapid fluctuations corresponding to a 3-day  $e$ -folding time scale. Superimposed upon these fluctuations is a positive trend. Therefore, the  $H$  index measures the day-to-day variation in the amplitude of the latent heating trend

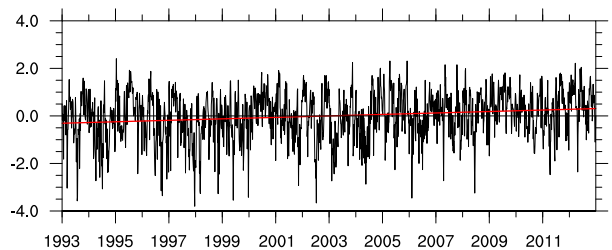


FIG. 3. The time series of the  $H$  index for 1993–2012. The red line indicates the linear trend of the DJF mean values of the  $H$  index.

pattern at its intrinsic 3-day time scale. We perform linear regressions of different variables against the daily  $H$  index. Furthermore, in addition to these rapid daily variations, the DJF mean values of the  $H$  index undergo a positive trend, as indicated by the red line in Fig. 3. Statistical significance of this trend was examined with a Mann–Kendall trend test. This trend is found to be statistically significant at the 99% level.

The regression equation between the variable of interest  $Y$ , such as latent heating, SAT, downward IR, and surface heat flux, and the  $H$  index, is

$$\Delta Y(\lambda, \theta) = [r\sigma(Y)/\sigma(H)] \Delta H, \quad (3)$$

where  $\Delta H$  is the interdecadal trend in the DJF-averaged values of the  $H$  index, and  $\Delta Y$  is the 1993–2012 linear interdecadal trend in  $Y$  at each grid point associated with the interdecadal trend in the  $H$  index. The quantity  $r$  is the linear correlation between the daily values of  $Y$  and the  $H$  index, with the DJF mean values of  $Y$  at each grid point and the  $H$  index subtracted for each winter, and  $\sigma(Y)$  and  $\sigma(H)$  are the standard deviations of  $Y$  and the  $H$  index, respectively, again with the DJF mean values subtracted. Therefore, the regression coefficient expresses the intraseasonal relationship between  $Y$  and the  $H$  index. Since the regression coefficient in (3) is multiplied by  $\Delta H$ ,  $\Delta Y$  in (3) corresponds to an estimate of the interdecadal trend in  $Y$  due to both its intraseasonal relationship with  $H$  index (i.e., the daily time series of the interdecadal latent heating trend pattern) and the interdecadal trend in the  $H$  index. It is important to mention that (3) is based on an a posteriori assumption. The validity of this assumption was examined by comparing the lag day 0 regressed latent heating pattern (see Fig. 7f) with the 1993–2012 latent heating trend pattern in Fig. 2. That is, we compare  $\Delta Y$  in (3) with the observed interdecadal trend in  $Y$ , where  $Y$  is the latent heating field. If  $\Delta Y$  does indeed resemble the observed interdecadal trend in  $Y$ , then a large fraction of the interdecadal trend in the latent heating arises from intraseasonal fluctuations in the latent heating field as represented by the daily  $H$  index. A comparison of this (see Fig. 7f) with the trend pattern in Fig. 2 shows that these two patterns are indeed similar. A calculation of the pattern correlation between these two latent heating trend patterns over the domain 30°W–60°E, 60°–90°N is found to be 0.71.

To investigate the intraseasonal and interdecadal relationship between the different variables  $Y$  and the  $H$  index, lead–lag regressions are performed over a range of time lags from 20 days before to 20 days after the  $H$  index peaks. For this purpose, we estimate the trend  $\Delta Y$  for 1993–2012 by computing the time-lagged regression

coefficient  $[r(\tau)\sigma(Y)/\sigma(H)]$  between  $Y$  and the  $H$  index at time lag  $\tau$ , and then multiplying the regression coefficient by the linear interdecadal trend in the  $H$  index. The form of this regression coefficient is identical to that in (3), except for the time lag. The intraseasonal lead–lag relationship between  $Y$  and the  $H$  index is determined by the values of the regression coefficient at time lag  $\tau$ . (It should be noted that the various time lags in Fig. 4, as well as the time lags in Figs. 5–8, which we will discuss below, illustrate the intraseasonal relationship between the variables shown in these figures and the  $H$  index.)

Next, we investigate the relationship between the latent heating trend pattern and the surface heat flux (sensible plus latent heat flux), surface downward IR, the vertical integral of the moisture flux convergence multiplied by latent heat of vaporization  $L$ , SAT, and sea ice concentration for various time lags (Fig. 4). At lag –12 days (lag –12 days corresponds to the variable  $Y$  leading the latent heating index by 12 days), it is found that the surface heat flux, downward IR, SAT, and moisture flux convergence are weak over most of the Arctic. At lag –6 days, as the circulation brings warm moist air into the Arctic from the northeast North Atlantic Ocean through the Greenland Sea, the downward IR and SAT both show similar positive anomalies over much of the Arctic. By lag 0 days, it can be seen that the anomalies in the downward IR continue to closely resemble those of the SAT over most of the Arctic, with these anomalies being most similar in spatial structure over the GBKS region, the same region as that with the largest latent heating trends for the 1993–2012 time period (Fig. 2). By lag +6 days, the downward IR and SAT positive anomalies have substantially decreased, indicating that the evolution of the downward IR and SAT take place on a relatively short time scale. Also, concurrent with the intensification of the positive downward IR and SAT anomalies over the northern GBKS, there is a positive surface heat flux anomaly, indicating that there is an anomalous heat transfer from the atmosphere to the surface over these seas. The downward heat flux builds up to its largest value at lag zero and then declines. By lag +6 days, for northern half of the GBKS, the sign of the surface heat flux changes and the surface heat flux turns upward. By lag +12 days, the surface heat flux is upward over the entire GBKS region.

To investigate the relationship between the latent heating and sea ice loss, we perform lagged regressions between GBKS averaged sea ice concentration and the  $H$  index (Fig. 5). If the latent heating generally results from sea ice loss, then one would expect negative sea ice anomalies to precede the latent heating maximum. At negative lags, no statistically significant values are found, and at positive lags, statistically significant negative values

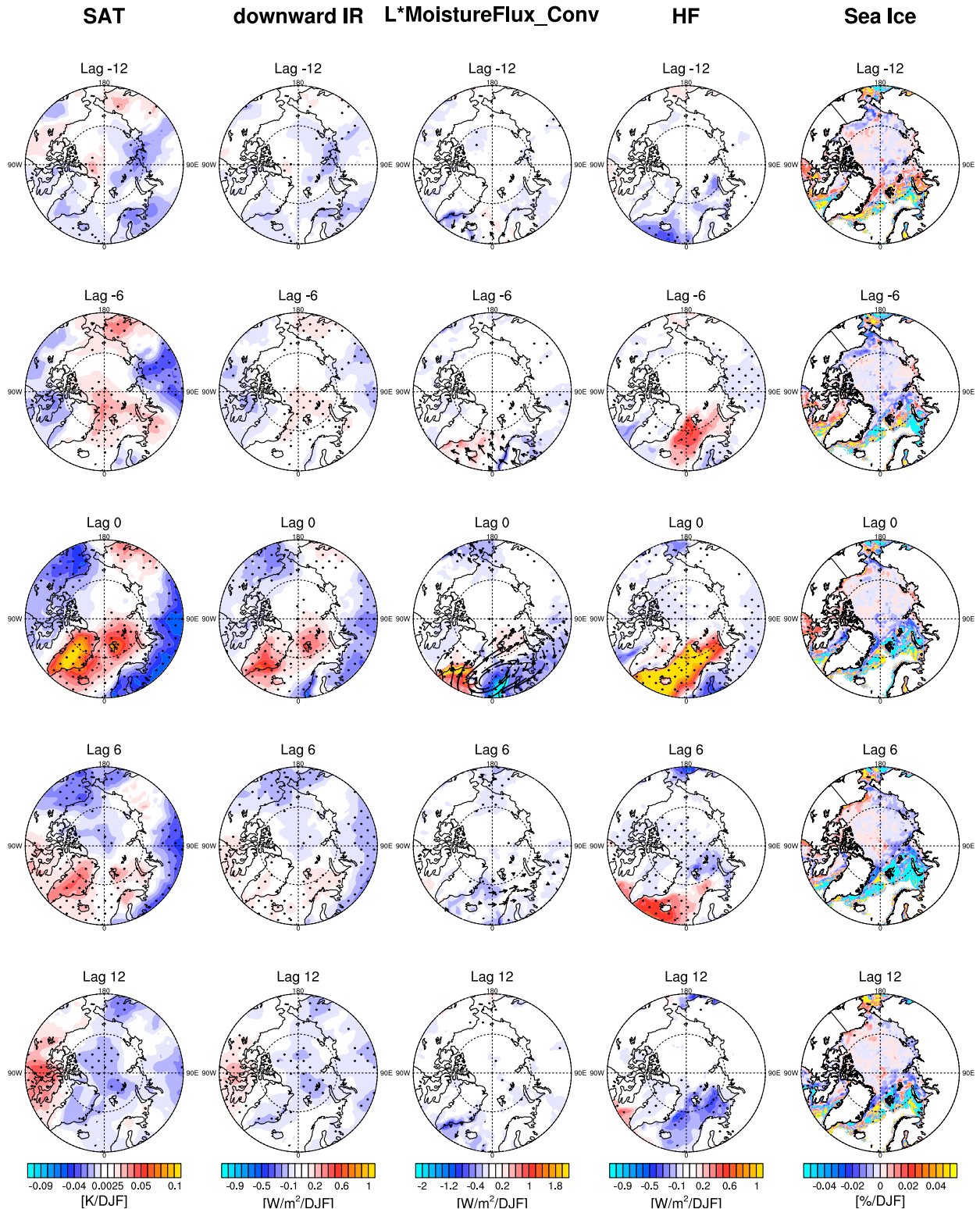


FIG. 4. The estimated trends for different variables obtained by multiplying the regression coefficients (regression against the  $H$  index) and the trend in the  $H$  index for 1993–2012. Trends are shown for (first column) the surface air temperature, (second column) the downward IR, (third column) the vertically integrated moisture flux vectors and moisture flux convergence multiplied by  $L$  ( $L*\text{MoisFluxconv}$ ), (fourth column) the surface heat flux, and (fifth column) the sea ice concentration. The corresponding lag is shown above each panel. The dots indicate values that are statistically significant at the  $p < 0.10$  level for a two-sided Student's  $t$  test (ERA-Interim dataset).

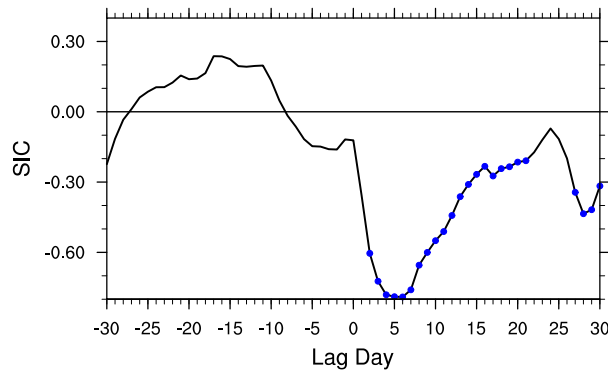


FIG. 5. The time evolution of the regressed SIC averaged over the GBKS region (30°W–90°E, 65°–85°N). The blue dots indicate values that are statistically significant at the  $p < 0.10$  level.

(corresponding to sea ice loss) are found peaking at lag +6 days. The GBKS sea ice minimum value at lag +6 days occurs about one week after the Rossby wave train first enters the Arctic.

The maximum correlation in Fig. 5, although statistically significant ( $p < 0.10$ ), has a value of  $-0.20$  (not shown). As shown in many studies (e.g., GFL; Gong and Luo 2017; H.-S. Park et al. 2015; D.-S. Park et al. 2015), there is a more direct relationship between sea ice melting and surface downward IR. Indeed, the corresponding maximum correlation between the downward IR index of GFL and GBKS sea ice area is larger, with a value of  $-0.49$ ; downward IR is influenced not only by latent heating, but also by poleward heat and moisture fluxes into the GBKS region. This result indicates that other processes, in addition to an increase in surface downward IR due to warm moist air intrusions associated with Rossby waves propagating from the midlatitudes into the Arctic, also contribute to the decline of GBKS sea ice. Recently, D.-S. Park et al. (2015) showed that sea ice drift and SST also contribute to the GBKS sea ice decline. Nevertheless, the relative small correlations do not impact the main thrust of this study—the question of whether Rossby wave trains propagating from the Arctic into midlatitudes are driven by in situ processes, or from a trans-Arctic wave train—because, as discussed in the introduction, it is the relative timing between the wave train and the anomalous latent heating, not sea ice area, that indicates whether the wave train is typically generated by in situ processes.

### c. Circulation pattern and wave activity flux

To investigate whether the latent heating over the Arctic is linked with Rossby wave propagation into and out of the Arctic, we computed the horizontal components of the wave activity flux vector (Takaya and Nakamura 2001) based on the regression of the 300-hPa

streamfunction against the daily  $H$  index for the entire Northern Hemisphere (Fig. 6). At lag  $-14$  days, a cyclonic streamfunction anomaly formed near the Philippine Sea centered at 35°N and 140°E, with a concurrent latent heating anomaly over the warm pool region (see Fig. 7). Sardeshmukh and Hoskins (1988) suggest that tropical convection can generate streamfunction anomalies in the subtropics via the so-called Rossby wave source, through the excitation of a divergent wind field that extends from the deep tropics into the subtropics. A calculation of the inverse Laplacian of the anomalous Rossby wave source finds that it overlays the cyclonic streamfunction anomaly centered at 140°E (not shown), which suggests that the cyclonic streamfunction anomaly is excited by tropical convection. As shown in the modeling study of Lukens et al. (2017), such a negative streamfunction anomaly is typically advected eastward by the subtropical jet, accounting for the location of the cyclonic streamfunction anomaly near the date line at lag  $-8$  days. By lag  $-8$  days, eastward wave activity flux vectors can be seen extending across the central subtropical Pacific from 150°E to 150°W, after which these wave activity flux vectors split into two directions, one with a southeastward orientation toward the equator and the other with a northeastward orientation toward higher latitudes over the North Pacific. These two groups of wave activity fluxes are associated with Rossby wave trains that can be identified by the 300-hPa streamfunction anomalies in Fig. 6, with the former wave train consisting of positive and negative anomalies that extend from the anomalous low over the date line into the eastern tropical Pacific. The direction of propagation of the former wave train can also be identified by the southwest/northeast tilt of the anomalous low over the date line (Hoskins and Karoly 1981). The second wave train extends from the same anomalous low northeastward toward high latitudes, that is, over the midlatitude North Pacific, Alaska, and Arctic Canada and then into the GBKS region. All the anomaly centers of the high-latitude wave train continue to strengthen over the following 4 days. A comparison of the streamfunction anomalies over the time interval from lag  $-4$  to lag  $+4$  days indicates that the lower-latitude anomalies weaken and the higher-latitude anomalies strengthen. Furthermore, over the same time interval, the lower-latitude wave activity flux vectors shorten and the high-latitude wave activity flux vectors lengthen. Therefore, even though wave activity can be seen entering the Arctic from the subtropical Pacific by lag  $-4$  days, the amplitude of the wave activity that enters and passes through the Arctic continues to strengthen after lag  $-4$  days. By lag 4 days (Fig. 6), the above high-latitude wave train pattern is observed to split into two branches, with one branch showing propagation eastward over the Barents and Kara Seas, through Eurasia toward



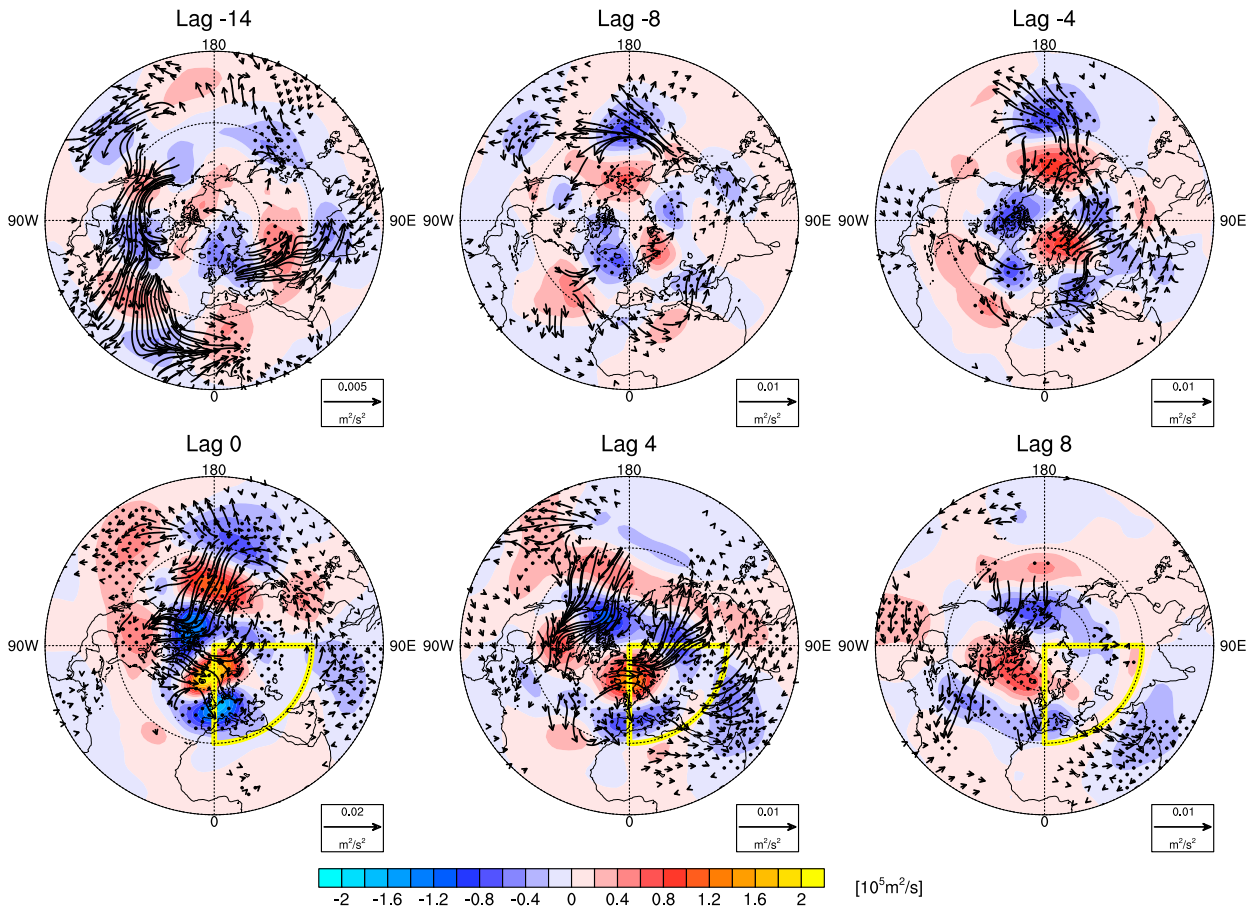


FIG. 6. The horizontal component of the wave activity flux (vectors) calculated from the regression of 300-hPa streamfunction (shading) against the  $H$  index for 1993–2012. The vectors displayed in each panel have an amplitude that exceeds  $2/3$  of the time averaged value at each grid point. The dots indicate values that are statistically significant at the  $p < 0.10$  level for a two-sided Student's  $t$  test (ERA-Interim dataset).

the northwest Pacific, and the other branch showing southward propagation into northern Africa (the presence of these two wave trains can be seen in both the streamfunction anomalies and the wave activity flux vectors).

An important question is to address is how much of the variance at each grid point can be explained by the trans-Arctic regression pattern shown in Fig. 6. To address this question, we have calculated the linear correlations between the daily 300-hPa streamfunction at each grid point and the daily  $H$  index. A wave train pattern similar to that shown in Fig. 6 is obtained (not shown), with the largest correlations being slightly larger than 0.5 and statistically significant ( $p < 0.10$ ). These values imply that other processes contribute to the variability at each grid point, such as variability arising from baroclinic instability, and wave train propagation from the tropics and the Arctic, the latter perhaps including the excitation of waves due to latent heating associated with sea ice melting. However, since we find that sea ice loss lags wave activity propagation into the

Arctic, our finding implies that if latent heat release associated with sea ice loss is playing a role, that role must be secondary, since that process is not evident in the lagged regressions.

#### d. Latent heating and moisture flux convergence

We next examine lagged regressions of the total latent heating against the daily  $H$  index. Previous research with observational data has suggested that a poleward propagating Rossby wave train resembling that shown in Fig. 6 over the North Pacific is often excited by tropical convection (e.g., Mori and Watanabe 2008; Johnson and Feldstein 2010; Moore et al. 2010; Lee et al. 2011). The presence of a positive latent heating anomaly at lag  $-14$  days in the western tropical Pacific shown in Fig. 7 suggests that this is indeed the case. At the same lag, a second region of positive anomalous latent heating can be seen in the central subtropical Pacific to the east of the date line. By lag  $-8$  days, the latent heating anomaly

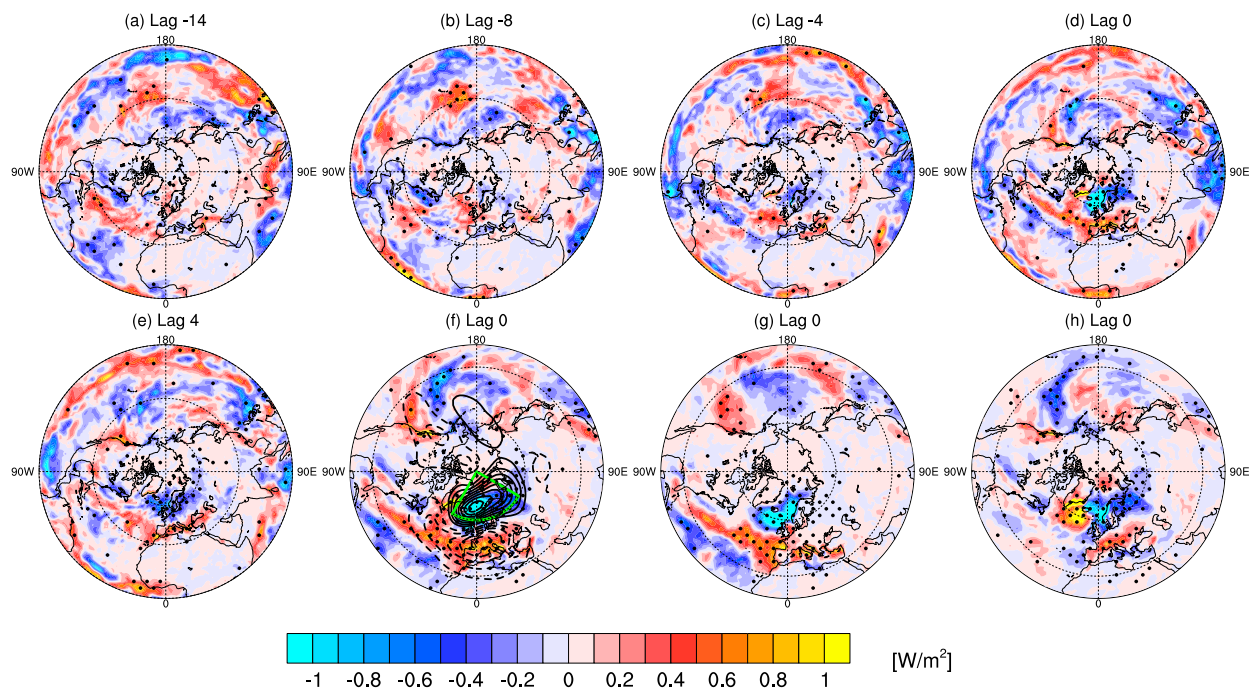


FIG. 7. (a)–(e) The estimated trends of the vertically integrated latent heating (shading) for 1993–2012 for the entire Northern Hemisphere. (f) The 700-hPa streamfunction (contours; the contour interval is  $2 \times 10^4 \text{ m}^2 \text{ s}^{-1}$ ) overlaid with the latent heating at lag 0 days and (g),(h) the convective and large-scale condensational heating, respectively, at lag 0 days, where (f)–(h) are shown for the domain poleward of  $20^\circ\text{N}$ . The dots indicate values that are statistically significant at the  $p < 0.10$  level for a two-sided Student's  $t$  test (JRA-55 dataset).

over the subtropical central Pacific has strengthened, followed by its gradual decay over the same location by lag  $-4$  days. By lag 0 days, poleward of  $60^\circ\text{N}$ , another region of positive anomalous latent heating develops that is centered over the northern GBKS region, as well as a region of negative anomalous latent heating over the southern GBKS, the Norwegian Sea, and the northeast North Atlantic (see the bottom row, second panel in Fig. 7, which highlights the latent heating anomalies over the GKBS region and nearby latitudes). This pattern of positive and negative anomalous latent heating in the GKBS region (indicated by the green box in Fig. 7f) resembles that associated with the latent heating trend in Fig. 2, consistent with our a posteriori assumption that much of the interdecadal variability over the Arctic is associated with intraseasonal latent heating fluctuations. By comparing the convective heating (Fig. 7g) and the large-scale condensational heating (Fig. 7h), it is found that the tropical and subtropical latent heating anomalies in Fig. 7 are mostly dominated by convective heating, and the over Arctic the two forms of latent heating are similar except over the high Arctic, where large-scale condensational heating dominates. In addition, as can be seen from Figs. 6 and 7, the wave amplifies after the maximum latent heating at lag 0 days. This relationship between

latent heat release and wave amplitude can be understood from Takaya and Nakamura (2001), who show that the wave activity tendency is proportional to the wave activity source (i.e., the latent heat release). Therefore, it is to be expected that the wave activity will amplify for several days after the maximum latent heat release. At lag  $+4$  days the same latent heating anomalies are present but with a much smaller amplitude. Also, since the surface heat fluxes over the GBKS region first become upward near lag  $+6$  days (Fig. 4) (the surface heat fluxes in the GBKS are still downward at lag  $+2$  and lag  $+4$  days; not shown), it is unlikely that a positive feedback associated with sea ice loss is having much influence on the equatorward propagating wave train, which is already evident at lag 0 days.

An examination of the lower tropospheric streamfunction and latent heating anomalies indicates spatial patterns that are consistent with the wave packet amplifying as it passes over the Norwegian and Barents Seas. Noting that there is a Rossby wave activity source when the streamfunction and latent heating anomalies are out of phase (Takaya and Nakamura 2001), it is seen that when positive and negative latent heating anomalies peak (i.e., at lag 0 days) there is marked overlap between the positive 700-hPa streamfunction anomaly (Fig. 7f, contours)

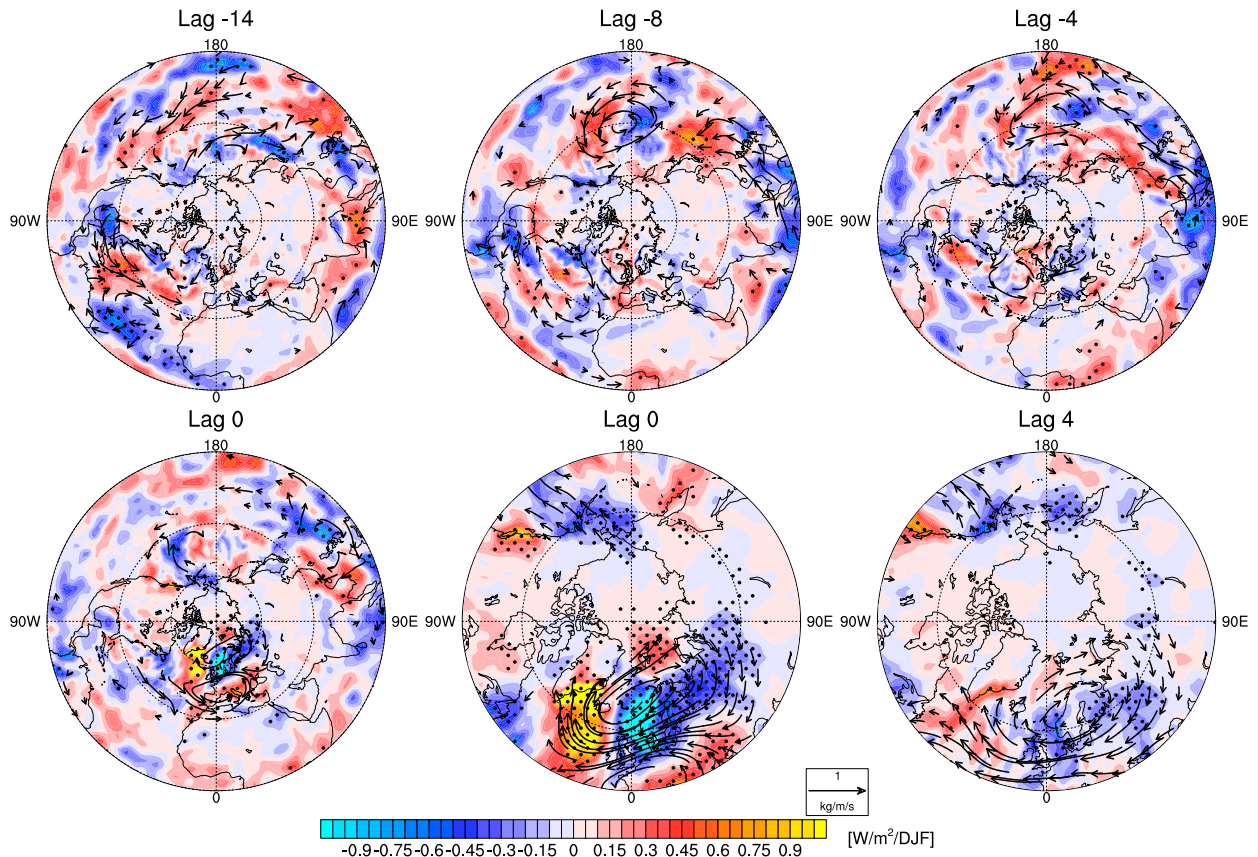


FIG. 8. The estimated trends of the vertically integrated moisture flux (vectors) and its convergence multiplied by  $L$  for the entire Northern Hemisphere, except the lower-middle and lower-right panels are for the domain poleward of  $45^{\circ}\text{N}$ . The dots indicate values that are statistically significant at the  $p < 0.10$  level for a two-sided Student's  $t$  test (ERA-Interim dataset).

and the negative latent heating anomaly (Fig. 7f, shading) over the southern GBKS region and the Norwegian Sea. This result is consistent with there being an important Rossby wave activity source (Takaya and Nakamura 2001) due to negative anomalous latent heating. Since the positive latent heating over the anomaly over the northern GBKS overlaps with small values of the streamfunction anomaly, it does not make an important contribution to the amplification of the trans-Arctic wave train. Over southwestern Europe, a positive latent heating anomaly and a negative streamfunction anomaly overlap. This latent heating anomaly results in further amplification of the wave train, but this amplification occurs outside of the Arctic.

Next, we investigate the corresponding changes of the moisture flux and its convergence associated with the Arctic latent heating. Figure 8 shows the lagged regressions of the vertically integrated moisture flux vector, and moisture flux convergence against the latent heating index. At lag  $-14$  days, over the central tropical Pacific (centered near  $15^{\circ}\text{N}$  between  $150^{\circ}\text{E}$  and  $150^{\circ}\text{W}$ ),

there are anomalous northeastward moisture fluxes that transport moist air into the subtropical central Pacific where there is convergence centered near  $22^{\circ}\text{N}$  and  $165^{\circ}\text{W}$ . By lag  $-8$  days, the cyclonic flow anomaly in the subtropical Pacific (Fig. 6) transports moisture eastward on its southern flank and westward on its northern flank. The eastward moisture flux is associated with a strong moisture flux convergence in the same general region as at lag  $-14$  days. The location of this moisture flux convergence at lag  $-8$  days closely overlaps with the positive latent heating anomaly in the same region also at lag  $-8$  days (Fig. 7). This finding suggests that the concurrent positive latent heating anomalies arises in part from moisture flux convergence. As the wave trains propagate toward high latitudes (Fig. 6, vectors), at lag  $-4$  days, both the subtropical latent heating (Fig. 7) and the moisture convergence (Fig. 8) diminish. By lag 0 days, the moisture flux vectors show two regions of convergence, one east of Greenland, and the other over the northern Barents Sea (see the lower right panel in Fig. 8). A region of moisture flux divergence can be seen

over the southern Barents Sea and the Norwegian Sea. These results also suggest that this anomalous moisture flux convergence/divergence contributes to the anomalous latent heating over the GBKS region. Furthermore, as implied by our calculations and shown in other studies (e.g., Zhong et al. 2018), moisture that has been advected into the Barents and Kara Seas was picked up from the North Atlantic by the poleward propagating wave train.

By comparing the spatial structure of the moisture flux vectors and the 300-hPa streamfunction anomalies (Fig. 6), it can be seen that the anticyclone centered over the GBKS region is crucial for transporting warm, moist air from the southern GBKS region, Norwegian Sea, and the northeast North Atlantic into the northern GBKS region, resulting in the above moisture flux convergence/divergence pattern. Because the anticyclone is part of the wave train that extends across the North Pacific, Alaska, and Arctic Canada, the moisture flux convergence/divergence over the GBKS region can be understood as being associated with part of the poleward propagating Rossby wave train. It is through this moisture flux convergence/divergence that there is an amplification of the trans-Arctic Rossby wave, which then propagates to the midlatitudes.

#### 4. Conclusions and discussion

In this study, we have examined the question of whether the excitation of equatorward propagating Rossby waves from the Arctic into midlatitudes is due to 1) in situ processes over the Arctic Ocean, of which sea ice loss and the subsequent upward flux of latent heat is one of several examples, or 2) Rossby waves propagating from midlatitudes into the Arctic and then back into midlatitudes, with these Rossby waves triggering the release of latent heat, which amplifies these waves as they pass through the Arctic. As discussed in the introduction, one important factor when addressing this question involves the relative timing between the wave train and anomalous latent heat release, since latent heat release can serve as a Rossby wave activity source. If 1) the anomalous Arctic latent heating is preceded by Rossby wave propagation into the Arctic, 2) the spatial structure of the anomalous Arctic latent heating is consistent with it being generated by the poleward propagating Rossby wave train, and 3) the anomalous Arctic latent heating is followed by equatorward Rossby wave propagation, then the Arctic latent heating is not associated with in situ processes; that is, we can claim that Arctic sea ice loss, as well other in situ processes that generate latent heating (see the above four examples in the introduction), cannot be the main driver of the equatorward propagating Rossby wave train.

By performing lagged regression calculations, we estimated the interdecadal trend in different atmospheric variables (i.e., Rossby wave activity flux, streamfunction, downward IR, SAT, surface heat flux, and column integrated moisture flux convergence) due to both its intra-seasonal relationship with the  $H$  index (i.e., the daily time series of the interdecadal latent heating trend pattern) and the interdecadal trend in the  $H$  index. It is shown that a poleward propagating Rossby wave train, which brings warm and moist air into the Arctic, is associated with anomalous latent heat release, and is followed by amplification of the wave train and then equatorward Rossby wave propagation. This finding implies that the Rossby wave propagation from the Arctic into midlatitudes primarily arises from trans-Arctic wave propagation, with other processes such as in situ wave generation playing a secondary role. With the linear regression method used in our study, we find that the correlation between the  $H$  index and the 300-hPa streamfunction field is 0.5, suggesting that the trans-Arctic wave train accounts for about 25% of the streamfunction variance. Although our method did not allow for determining the variance explained by in situ wave generation, the fact that the trans-Arctic wave train dominates the streamfunction field regressed onto the  $H$  index indicates that the variance associated with the trans-Arctic wave train must be greater than that of in situ wave generation.

By regressing the above variables against the latent heating index, we also show that the poleward propagating Rossby wave train is preceded by latent heating in the tropics. Using reanalysis data, Yoo et al. (2011) showed that there has been an interdecadal increase in the frequency of Madden-Julian oscillation phases 4–6, which coincide with an increase in the frequency of warm pool tropical convection, poleward propagation of Rossby waves from the subtropics to the Arctic, and an increase in Arctic SAT. Using an idealized multilevel primitive equation model, Yoo et al. (2012) showed that Rossby waves excited by tropical latent heating advect a passive tracer from the midlatitudes into the Arctic. Taken together, these papers suggest that the latent heating trend has its source in an increase in the frequency of warm pool tropical convection, which results in an increase in the frequency of poleward propagating Rossby waves and the moisture flux convergence/divergence associated with these Rossby waves, and then anomalous latent heating in the Arctic.

Previous studies have also shown that Arctic amplification and the melting of Arctic sea ice during the winter is associated with poleward propagating Rossby wave trains that were excited by warm pool tropical convection (Lee 2014; H.-S. Park et al. 2015; Goss et al. 2016; Baggett and Lee 2017). This process has been referred

to as the tropically excited Arctic warming (TEAM) mechanism. The TEAM mechanism been shown to operate on a wide range of time scales, including that associated with the intraseasonal Madden–Julian oscillation (Yoo et al. 2012), the interannual El Niño–Southern Oscillation (Lee 2012), and the much longer interdecadal trend (Lee et al. 2011). In this study, the regression calculations suggest that the poleward propagating Rossby waves are excited via a two-step process that involves convective heating in both the warm pool and the central subtropical Pacific. The warm pool convective heating appears to excite a cyclonic streamfunction anomaly in the western subtropical Pacific as evidenced by the occurrence of a cyclonic Rossby wave source anomaly in the same region. This cyclonic streamfunction anomaly propagates eastward into the central subtropical Pacific where a pre-existing convective anomaly is likely enhanced by the cyclonic streamfunction anomaly. This heating anomaly coincides with moisture flux convergence associated with the cyclonic streamfunction anomaly. The same relationship between the warm pool and subtropical convective heating has been found in association with the Pacific–North American teleconnection pattern (Dai et al. 2017). This result hints at the possibility that a similar two-step process occurs for the TEAM mechanism on the interannual and interdecadal time scales.

The horizontal components of the wave activity fluxes revealed a Rossby wave train that propagates poleward from the subtropical central Pacific, into the Arctic, and then back into midlatitudes. This wave train is associated with latent heating anomalies over the GBKS region. The moisture flux convergence (divergence) anomalies coincide with positive (negative) latent heating anomalies, suggesting that the anticyclonic streamfunction anomaly within the wave train over the Arctic generates the latent heating anomalies via moisture flux convergence/divergence, in analogy with the latent heating anomaly in the central subtropical Pacific. In addition, because the negative latent heating anomaly overlaps with an anomalous high over the Arctic, it appears that this latent heating anomaly fuels the Rossby wave train that transits the Arctic and propagates back into midlatitudes. Therefore, we conclude that it is useful to describe the entire wave train as trans-Arctic wave train recharged over the Arctic.

*Acknowledgments.* The ERA-Interim data used in this study were downloaded from the ECMWF data server. We thank Dr. Doug Smith for his helpful discussion on the atmospheric response to sea ice loss in climate models. We also thank three anonymous reviewers whose comments were very beneficial. This study was supported by the National Natural Science Foundation of China

(41875073, 41790473), and National Science Foundation Grants AGS-1455577, AGS-1401220, AGS-1822015, and OPP-1723832.

## REFERENCES

- Alekseev, G., S. Kuzmina, L. Bobylev, A. Urazgildeeva, and N. Gnatiuk, 2019: Impact of atmospheric heat and moisture transport on the Arctic warming. *Int. J. Climatol.*, **39**, 3582–3592, <https://doi.org/10.1002/joc.6040>.
- Alexander, M. A., R. Tomas, C. Deser, and D. M. Lawrence, 2010: The atmospheric response to projected terrestrial snow changes in the late twenty-first century. *J. Climate*, **23**, 6430–6437, <https://doi.org/10.1175/2010JCLI3899.1>.
- Baggett, C., and S. Lee, 2017: An identification of the mechanisms that lead to Arctic warming during planetary-scale and synoptic-scale wave life cycles. *J. Atmos. Sci.*, **74**, 1859–1877, <https://doi.org/10.1175/JAS-D-16-0156.1>.
- Bekryaev, R. V., I. V. Polyakov, and V. A. Alexeev, 2010: Role of polar amplification in long-term surface air temperature variations and modern Arctic warming. *J. Climate*, **23**, 3888–3906, <https://doi.org/10.1175/2010JCLI3297.1>.
- Budikova, D., 2009: Role of Arctic sea ice in global atmospheric circulation: A review. *Global Planet. Change*, **68**, 149–163, <https://doi.org/10.1016/j.gloplacha.2009.04.001>.
- Cavalieri, D. J., C. L. Parkinson, P. Gloersen, and H. J. Zwally, 1996: Sea ice concentrations from Nimbus-7 SMMR and DMSP SSM/I passive microwave data. National Snow and Ice Data Center, accessed 2017, <https://doi.org/10.5067/8GQ8LZQVL0VL>.
- Chapman, W. L., and J. E. Walsh, 1993: Recent variations of sea ice and air temperature in high latitudes. *Bull. Amer. Meteor. Soc.*, **74**, 33–48, [https://doi.org/10.1175/1520-0477\(1993\)074<0033:RVOSIA>2.0.CO;2](https://doi.org/10.1175/1520-0477(1993)074<0033:RVOSIA>2.0.CO;2).
- Clark, J. P., and S. B. Feldstein, 2020: What drives the North Atlantic Oscillation's surface air temperature anomaly pattern? Part I: The growth and decay of the surface air temperature anomalies. *J. Atmos. Sci.*, **77**, 185–198, <https://doi.org/10.1175/JAS-D-19-0027.1>.
- Cohen, J., and Coauthors, 2014: Recent Arctic amplification and extreme mid-latitude weather. *Nat. Geosci.*, **7**, 627–637, <https://doi.org/10.1038/ngeo2234>.
- Dai, Y., S. B. Feldstein, B. Tan, and S. Lee, 2017: Formation mechanisms of the Pacific–North American teleconnection with and without its canonical tropical convection pattern. *J. Climate*, **30**, 3139–3155, <https://doi.org/10.1175/JCLI-D-16-0411.1>.
- Dee, D. P., and Coauthors, 2011: The ERA-Interim reanalysis: Configuration and performance of the data assimilation system. *Quart. J. Roy. Meteor. Soc.*, **137**, 553–597, <https://doi.org/10.1002/qj.828>.
- Deser, C., R. A. Tomas, and S. Peng, 2007: The transient atmospheric circulation response to North Atlantic SST and sea ice anomalies. *J. Climate*, **20**, 4751–4767, <https://doi.org/10.1175/JCLI4278.1>.
- , —, M. Alexander, and D. Lawrence, 2010: The seasonal atmospheric response to projected Arctic sea ice loss in the late twenty-first century. *J. Climate*, **23**, 333–351, <https://doi.org/10.1175/2009JCLI3053.1>.
- , L. Terray, and A. S. Phillips, 2016: Forced and internal components of winter air temperature trends over North America during the past 50 years: Mechanisms and implications. *J. Climate*, **29**, 2237–2258, <https://doi.org/10.1175/JCLI-D-15-0304.1>.

- Ding, Q., and Coauthors, 2017: Influence of high-latitude atmospheric circulation changes on summertime Arctic sea ice. *Nat. Climate Change*, **7**, 289–295, <https://doi.org/10.1038/nclimate3241>.
- Doyle, J. G., G. Lesins, C. P. Thackray, C. Perro, G. J. Nott, T. J. Duck, R. Damoah, and J. R. Drummond, 2011: Water vapor intrusions into the high Arctic during winter. *Geophys. Res. Lett.*, **38**, L12806, <https://doi.org/10.1029/2011GL047493>.
- Ebita, A., and Coauthors, 2011: The Japanese 55-year reanalysis “JRA-55”: An interim report. *Sci. Online Lett. Atmos.*, **7**, 149–152, <https://doi.org/10.2151/sola.2011-038>.
- Feldstein, S. B., 2003: The dynamics of NAO teleconnection pattern growth and decay. *Quart. J. Roy. Meteor. Soc.*, **129**, 901–924, <https://doi.org/10.1256/QJ.02.76>.
- , and S. Lee, 2014: Intraseasonal and interdecadal jet shifts in the Northern Hemisphere: The role of warm pool tropical convection and sea ice. *J. Climate*, **27**, 6497–6518, <https://doi.org/10.1175/JCLI-D-14-00057.1>.
- Francis, J. A., and S. J. Vavrus, 2012: Evidence linking Arctic amplification to extreme weather in mid-latitudes. *Geophys. Res. Lett.*, **39**, L06801, <https://doi.org/10.1029/2012GL051000>.
- , and —, 2015: Evidence for a wavier jet stream in response to rapid Arctic warming. *Environ. Res. Lett.*, **10**, 014005, <https://doi.org/10.1088/1748-9326/10/1/014005>.
- Gong, T., and D. Luo, 2017: Ural blocking as an amplifier of the Arctic sea ice decline in winter. *J. Climate*, **30**, 2639–2654, <https://doi.org/10.1175/JCLI-D-16-0548.1>.
- , S. Feldstein, and S. Lee, 2017: The role of downward infrared radiation in the recent Arctic winter warming trend. *J. Climate*, **30**, 4937–4949, <https://doi.org/10.1175/JCLI-D-16-0180.1>.
- Goss, M., S. B. Feldstein, and S. Lee, 2016: Stationary wave interference, and its relation to tropical convection and Arctic warming. *J. Climate*, **29**, 1369–1389, <https://doi.org/10.1175/JCLI-D-15-0267.1>.
- Honda, M., J. Inoue, and S. Yamane, 2009: Influence of low Arctic sea-ice minima on anomalously cold Eurasian winters. *Geophys. Res. Lett.*, **36**, L08707, <https://doi.org/10.1029/2008GL037079>.
- Hoskins, B. J., and D. J. Karoly, 1981: The steady linear response of a spherical atmosphere to thermal and orographic forcing. *J. Atmos. Sci.*, **38**, 1179–1196, [https://doi.org/10.1175/1520-0469\(1981\)038<1179:TSLROA>2.0.CO;2](https://doi.org/10.1175/1520-0469(1981)038<1179:TSLROA>2.0.CO;2).
- Johnson, N. C., and S. B. Feldstein, 2010: The continuum of North Pacific sea level pressure patterns: Intraseasonal, interannual, and interdecadal variability. *J. Climate*, **23**, 851–867, <https://doi.org/10.1175/2009JCLI3099.1>.
- Kim, B.-M., S.-W. Son, S.-K. Min, J.-H. Jeong, S.-J. Kim, X. Zhang, T. Shim, and J.-H. Yoon, 2014: Weakening of the stratospheric polar vortex by Arctic sea-ice loss. *Nat. Commun.*, **5**, 4646, <https://doi.org/10.1038/ncomms5646>.
- Kobayashi, S., and Coauthors, 2015: The JRA-55 Reanalysis: General specifications and basic characteristics. *J. Meteor. Soc. Japan*, **93**, 5–48, <https://doi.org/10.2151/jmsj.2015-001>.
- Lee, H. J., M. O. Kwon, S.-W. Yeh, Y.-O. Kwon, W. Park, J.-H. Park, Y.-H. Kim, and M. A. Alexander, 2017: Impact of poleward moisture transport from the North Pacific on the acceleration of sea ice loss in the Arctic since 2002. *J. Climate*, **30**, 6757–6769, <https://doi.org/10.1175/JCLI-D-16-0461.1>.
- Lee, S., 2012: Testing of the tropically excited Arctic warming (TEAM) mechanism with traditional El Niño and La Niña. *J. Climate*, **25**, 4015–4022, <https://doi.org/10.1175/JCLI-D-12-00055.1>.
- , 2014: A theory for polar amplification from a general circulation perspective. *Asia-Pac. J. Atmos. Sci.*, **50**, 31–43, <https://doi.org/10.1007/S13143-014-0024-7>.
- , T. Gong, N. C. Johnson, S. B. Feldstein, and D. Pollard, 2011: On the possible link between tropical convection and the Northern Hemisphere Arctic surface air temperature change between 1958 and 2001. *J. Climate*, **24**, 4350–4367, <https://doi.org/10.1175/2011JCLI4003.1>.
- , —, S. B. Feldstein, J. Screen, and I. Simmonds, 2017: Revisiting the cause of the 1989–2009 Arctic surface warming using the surface energy budget: Downward infrared radiation dominates the surface fluxes. *Geophys. Res. Lett.*, **44**, 10 654–10 661, <https://doi.org/10.1002/2017GL075375>.
- Lukens, K. E., S. B. Feldstein, C. Yoo, and S. Lee, 2017: The dynamics of the extratropical response to Madden-Julian oscillation convection. *Quart. J. Roy. Meteor. Soc.*, **143**, 1095–1106, <https://doi.org/10.1002/qj.2993>.
- Luo, B., L. Wu, D. Luo, A. Dai, and I. Simmonds, 2019: The winter midlatitude–Arctic interaction: Effects of North Atlantic SST and high-latitude blocking on Arctic sea ice and Eurasian cooling. *Climate Dyn.*, **52**, 2981–3004, <https://doi.org/10.1007/s00382-018-4301-5>.
- Moore, R. W., O. Martius, and T. Spengler, 2010: The modulation of the subtropical and extratropical atmosphere in the Pacific basin in response to the Madden-Julian oscillation. *Mon. Wea. Rev.*, **138**, 2761–2779, <https://doi.org/10.1175/2010MWR3194.1>.
- Mori, M., and M. Watanabe, 2008: The growth and triggering mechanisms of the PNA: A MJO–PNA coherence. *J. Meteor. Soc. Japan*, **86**, 213–236, <https://doi.org/10.2151/jmsj.86.213>.
- Overland, J., and M. Wang, 2010: Large-scale atmospheric circulation changes are associated with the recent loss of Arctic sea ice. *Tellus*, **62A**, 1–9, <https://doi.org/10.1111/J.1600-0870.2009.00421.X>.
- , J. Francis, R. Hall, E. Hana, S. Kim, and T. Vihma, 2015: The melting Arctic and midlatitude weather patterns: Are they connected? *J. Climate*, **28**, 7917–7932, <https://doi.org/10.1175/JCLI-D-14-00822.1>.
- Park, D.-S. R., S. Lee, and S. B. Feldstein, 2015: Attribution of the recent winter sea-ice decline over the Atlantic sector of the Arctic Ocean. *J. Climate*, **28**, 4027–4033, <https://doi.org/10.1175/JCLI-D-15-0042.1>.
- Park, H.-S., S. Lee, S.-W. Son, S. B. Feldstein, and Y. Kosaka, 2015: The impact of poleward moisture and sensible heat flux on Arctic winter sea ice variability. *J. Climate*, **28**, 5030–5040, <https://doi.org/10.1175/JCLI-D-15-0074.1>.
- Peings, Y., and G. Magnusdottir, 2014: Response of the wintertime Northern Hemisphere atmospheric circulation to current and projected Arctic sea ice decline: A numerical study with CAM5. *J. Climate*, **27**, 244–264, <https://doi.org/10.1175/JCLI-D-13-00272.1>.
- Persson, P. O. G., C. W. Fairall, E. L. Andreas, P. S. Guest, and D. K. Perovich, 2002: Measurements near the atmospheric surface flux group tower at SHEBA: Near surface conditions and surface energy budget. *J. Geophys. Res.*, **107**, 8045, <https://doi.org/10.1029/2000JC000705>.
- Sardeshmukh, P. D., and B. J. Hoskins, 1988: The generation of global rotational flow by steady idealized tropical divergence. *J. Atmos. Sci.*, **45**, 1228–1251, [https://doi.org/10.1175/1520-0469\(1988\)045<1228:TGOGRF>2.0.CO;2](https://doi.org/10.1175/1520-0469(1988)045<1228:TGOGRF>2.0.CO;2).
- Screen, J. A., and I. Simmonds, 2013: Exploring links between Arctic amplification and mid-latitude weather. *Geophys. Res. Lett.*, **40**, 959–964, <https://doi.org/10.1002/grl.50174>.
- Sellers, W. D., 1969: A global climate model based on the energy balance of the Earth–atmosphere system. *J. Appl. Meteor.*, **8**, 392–400, [https://doi.org/10.1175/1520-0450\(1969\)008<0392:AGCMBO>2.0.CO;2](https://doi.org/10.1175/1520-0450(1969)008<0392:AGCMBO>2.0.CO;2).
- Serreze, M. C., J. D. Kahl, and R. C. Schnell, 1992: Low-level temperature inversions of the Eurasian Arctic and comparisons with

- Soviet drifting station data. *J. Climate*, **5**, 615–629, [https://doi.org/10.1175/1520-0442\(1992\)005<0615:LLTIOT>2.0.CO;2](https://doi.org/10.1175/1520-0442(1992)005<0615:LLTIOT>2.0.CO;2).
- , A. P. Barrett, J. C. Stroeve, D. N. Kindig, and M. M. Holland, 2009: The emergence of surface-based Arctic amplification. *Cryosphere*, **3**, 11–19, <https://doi.org/10.5194/tc-3-11-2009>.
- Sorokina, S. A., C. Li, J. J. Wettstein, and N. G. Kvamstø, 2016: Observed atmospheric coupling between Barents Sea ice and the warm-Arctic cold-Siberian anomaly pattern. *J. Climate*, **29**, 495–511, <https://doi.org/10.1175/JCLI-D-15-0046.1>.
- Sun, L., J. Perlwitz, and M. Hoerling, 2016: What caused the recent “Warm Arctic, Cold Continents” trend pattern in winter temperatures? *Geophys. Res. Lett.*, **43**, 5345–5352, <https://doi.org/10.1002/2016GL069024>.
- Takaya, K., and H. Nakamura, 2001: A formulation of a phase-independent wave-activity flux for stationary and migratory quasigeostrophic eddies on a zonally varying basic flow. *J. Atmos. Sci.*, **58**, 608–627, [https://doi.org/10.1175/1520-0469\(2001\)058<0608:AFOAPI>2.0.CO;2](https://doi.org/10.1175/1520-0469(2001)058<0608:AFOAPI>2.0.CO;2).
- Vihma, T., 2014: Effects of Arctic sea ice decline on weather and climate: A review. *Surv. Geophys.*, **35**, 1175–1214, <https://doi.org/10.1007/s10712-014-9284-0>.
- Walsh, J. E., 2014: Intensified warming of the Arctic: Causes and impacts on middle latitudes. *Global Planet. Change*, **117**, 52–63, <https://doi.org/10.1016/j.gloplacha.2014.03.003>.
- Woods, C., and R. Caballero, 2016: The role of moist intrusions in winter Arctic warming and sea ice decline. *J. Climate*, **29**, 4473–4485, <https://doi.org/10.1175/JCLI-D-15-0773.1>.
- , —, and G. Svensson, 2013: Large-scale circulation associated with moisture intrusions into the Arctic during winter. *Geophys. Res. Lett.*, **40**, 4717–4721, <https://doi.org/10.1002/grl.50912>.
- Woollings, T., B. Harvey, and G. Masato, 2014: Arctic warming, atmospheric blocking and cold European winters in CMIP5 models. *Environ. Res. Lett.*, **9**, 014002, <https://doi.org/10.1088/1748-9326/9/1/014002>.
- Yoo, C., S. Feldstein, and S. Lee, 2011: Impact of the Madden–Julian Oscillation (MJO) trend on the polar amplification of surface air temperature during 1979–2008 boreal winter. *Geophys. Res. Lett.*, **38**, L24804, <https://doi.org/10.1029/2011GL049881>.
- , S. Lee, and S. Feldstein, 2012: The impact of the Madden–Julian oscillation trend on the Antarctic warming during the 1979–2008 austral winter. *Atmos. Sci. Lett.*, **13**, 194–199, <https://doi.org/10.1002/asl.379>.
- Zhong, L., L. Hua, and D. Luo, 2018: Local and external moisture sources for the Arctic warming over the Barents-Kara Seas. *J. Climate*, **31**, 1963–1982, <https://doi.org/10.1175/JCLI-D-17-0203.1>.